QUASI-ELASTIC LIGHT-SCATTERING STUDIES OF SINGLE SKELETAL MUSCLE FIBERS

R. C. HASKELL AND F. D. CARLSON, *The Thomas C. Jenkins Department of Biophysics, The Johns Hopkins University, Baltimore, Maryland 21218 U.S.A.*

ABSTRACT Measurements were made of the intensity autocorrelation function, $g^{(2)}[\tau]$, of light scattered from intact frog muscle fibers. During the tension plateau of an isometric tetanus, scattered field statistics were approximately Gaussian and intensity fluctuations were quasi-stationary. The half time, $\tau_{1/2}$, for the decay of $g^{(2)}[\tau]$ was typically 70 ms at a scattering angle of 30°. The decay rate, $1/\tau_{1/2}$, of $g^{(2)}[\tau]$ varied roughly linearly with the projection of the scattering vector on the fiber axis. $1/\tau_{1/2}$ was greater during the tension creep phase of tetani of highly stretched fibers, but was roughly independent of sarcomere length during the tension plateau. $g^{(2)}[\tau]$ measured during rest or on diffraction pattern maxima during isometric contraction were flat with low amplitudes. These results are consistent with a model of a 200-μm segment of an isometrically contracting fiber in which scattering material possesses relative axial velocities of 1–2 μm/s accompanied by relative axial displacements >0.1 μm. The slow (1–2 μm/s) motion of one portion of the fiber relative to another observed under the microscope (500×) during isometric contraction is consistent with the light-scattering results. Structural fluctuations on the scale of the myofibrillar sarcomere which may arise from asynchronous cycling of cross-bridges must involve relative axial velocities <3 μm/s or relative axial displacements <0.05 μm.

INTRODUCTION

The sliding filament model of muscle contraction has been generally accepted for over 20 years (1–3). The structural integrity of the actin thin filaments and myosin thick filaments during tension generation has been observed in studies employing the optical microscope (1, 2) and x-ray diffraction (4, 5). The observation that the magnitude of tension developed by a single intact muscle fiber is proportional to the amount of overlap of thick and thin filaments implies that the sites of tension generation are uniformly distributed along the overlap region (6, 7). Low angle x-ray diffraction patterns of isometrically contracting muscle have been interpreted in terms of a molecular model for contracting muscle in which myosin cross-bridges cycle independently through attachment to actin filaments, tension generation, and detachment from actin (4, 5). The search for corroborating evidence for independent cycling of cross-bridges has led to the measurement of fluctuations in tension (8) and polarized fluorescence (9) in isometrically contracting preparations of glycerinated rabbit psoas fibers. Quasi-elastic light scattering has been used to search for structural fluctuations due to independently cycling cross-bridges in contracting muscle. Studies of whole sartorius muscle and fiber bundles of semitendinosus muscle of the frog have been reported by Bonner and

---

Dr. Haskell's present address is Physics Department, Harvey Mudd College, Claremont, Calif. 91711.

Carlson (10), and an analysis of the possible origin of the observed decay of the intensity autocorrelation function measured during isometric contraction was given by Carlson (11). This paper reports quasi-elastic light-scattering studies of single intact muscle fibers during isometric contraction.

Technique

Quasi-elastic light scattering, sometimes called intensity fluctuation spectroscopy (IFS) or photon correlation spectroscopy, has been used to investigate biological macromolecules and macromolecular systems for more than 10 years (12). Several excellent reviews, proceedings of conferences, and books dealing with this light-scattering technique have been published (13–16). Hence only an intuitive description of IFS will be given here. When a collimated beam of light coherently illuminates matter contained in a scattering volume, some of the light will be scattered out of the main beam due to the presence of optical inhomogeneities (scatterers). The polarizabilities, the spatial dimensions, and the spatial distribution of these scatterers at a particular time t determine the angular distribution of intensity $I(\theta, t)$ of the scattered light. If the polarizabilities and relative positions of the scatterers are constant in time, the scattered intensity at a given angle is constant. If, however, the polarizabilities or the relative positions fluctuate with time, the scattered intensity fluctuates on a time scale determined by the scattering angle and the dynamics of the fluctuations of the scattering material.

The temporal fluctuations in the scattered intensity can be characterized quantitatively by the intensity autocorrelation function defined by

$$G^{(2)}(\tau) = \langle I(t) \cdot I(t + \tau) \rangle,$$

where the brackets indicate a time average over the duration of an experiment. It is convenient to measure the normalized intensity autocorrelation function defined by

$$g^{(2)}(\tau) = G^{(2)}(\tau)/\langle I \rangle^2,$$

which in photocounting experiments becomes

$$g^{(2)}(\tau) = \langle n(t) \cdot n(t + \tau) \rangle / \langle n \rangle^2 \qquad \tau \neq 0,$$

where $n(t)$ and $n(t + \tau)$ are the numbers of photons recorded in time intervals of duration T (sample times) centered at t and $t + \tau$, respectively, and $\langle n \rangle$ is the average number of counts per sample time. Typically, an experiment consists of many contiguous sample times. The magnitude of the fluctuations of the scattered intensity about its mean value is described by the amplitude of the normalized intensity autocorrelation function

$$A = g^{(2)}(0) - 1 = \langle I^2 \rangle / \langle I \rangle^2 - 1 = \mathrm{Var}(I)/\langle I \rangle^2.$$

If scatterers execute relative displacements larger than the reciprocal of the scattering vector (typically 0.1 μm in these studies), the amplitude is roughly 1.0, so that the fluctuations of the scattered intensity are roughly equal to its mean value. If relative displacements are considerably smaller than the reciprocal of the scattering vector, the displacements are too small to be resolved with this light-scattering technique, and no significant intensity fluctuations will result.

In interpreting measurements of $g^{(2)}[\tau]$, it is instructive to compare the measured $g^{(2)}[\tau]$ with the $g^{(2)}[\tau]$ calculated from various relevant model systems. For a particular model, it is convenient to calculate first the normalized field autocorrelation function

$$g^{(1)}(\tau) = \langle E_s^*(t)E_s(t+\tau)\rangle / \langle I\rangle,$$

where $E_s(t)$ is the scattered electric field at time t. If $E_s(t)$ is Gaussian distributed in time with zero mean, $g^{(2)}[\tau]$ is simply related to $g^{(1)}(\tau)$ by

$$g^{(2)}[\tau] = 1 + |g^{(1)}(\tau)|^2.$$

When many independent scatterers are present in the scattering volume, the central limit theorem assures Gaussian field statistics. For example, when the scattering volume contains many freely diffusing identical Rayleigh scatterers,

$$g^{(1)}(\tau) = \exp[i\omega_0\tau] \exp[-\tau/\tau_{COH}],$$

and

$$g^{(2)}(\tau) = 1 + \exp[-2\tau/\tau_{COH}],$$

where ω_0 is the frequency of the incident light. The field coherence time, τ_{COH}, is a measure of the time scale of fluctuations in the scattered field and is determined by the translational diffusion constant of the scatterers and the scattering angle.

Summary

The optical inhomogeneities responsible for the scattering of light from a muscle fiber are primarily the contractile proteins. While 30% of the protein in a fiber is present as water soluble protein in the sarcoplasm (17, 18), the filament structure of the contractile proteins endows them with considerably more scattering power. The cross-bridges (HMM-S1 and S2) represent 35% of the contractile protein. However, since cross-bridge displacements are expected to be on the order of 0.01 μm, which is much less than the reciprocal of the scattering vector (0.1 μm), intensity fluctuations resulting directly from cross-bridge motion during isometric contraction can be expected to be <1% of the mean intensity. Nevertheless, Carlson (11) has pointed out that independent cycling of cross-bridges could lead to imbalances in the forces acting upon thick and thin filaments or myofibrillar A and I bands. With sufficient structural flexibility at the M or Z lines within myofibrillar A and I bands or at the interfaces between myofibrils, these force imbalances could lead to relative displacements comparable to the reciprocal of the scattering vector.

The measurements of $g^{(2)}(\tau)$ reported here revealed relative axial velocities of scattering material of 1–2 μm/s accompanied by relative axial displacements >0.1 μm. These results are consistent with the slow (1–2 μm/s) motion of one portion of the fiber with respect to another observed under the microscope (500×) during isometric contraction. This intrafiber motion possessed a correlation length of many micrometers (the motion of adjacent myofibrillar sarcomeres was highly correlated). Fig. 3 is a sketch of this type of motion observed during the tension plateau of a 2-s tetanus. While the possibility of structural fluctuations on the scale of the myofibrillar sarcomere cannot be excluded, an upper limit of 3 μm/s may be placed on relative axial velocities involving relative axial displacements >0.05 μm.

PREPARATION, APPARATUS, AND PROCEDURE

Preparation

Single fibers were dissected from the dorsal head of the semitendinosus muscle of southern grass frogs (*Rana pipiens*). The frogs had a body length of 7 cm, were stored at room temperature, and were used within 2 wk after their capture. Fibers were isolated at 10°C using stainless steel razor blades as described by Gordon et al. (7). Ringer's solution contained 110 mM NaCl, 2.3 mM KCl, 1.7 mM $CaCl_2$, 3.4 mM Na_2HPO_4, 1.4 mM NaH_2PO_4 (pH = 7.2), and 10^{-5} gm/ml tubocurarine. Fiber length when just taut was ~11 mm, which corresponded to a sarcomere length of 2.1 μm. Fiber diameters ranged from 50 to 120 μm. Attachment to the tendons was made with clips of 25-μm thick aluminum foil as described by Ford et al. (19). Holes made in the aluminum foil clips accepted hooks made of platinum wire of 0.5 mm diam.

Experimental Chamber

The dissection chamber served also as a testing, examination, and light-scattering chamber. The chamber was made of plexiglass and had a volume of 40 ml. The bottom of the chamber had a window made from a photographic slide. A separate lid had a similar window and mounted to the chamber with an o-ring seal. Filtered Ringer's solution was circulated through the chamber by means of glass tubing which passed through the chamber walls. The platinum hook at the tip of a rotatable finger slipped through the hole of the aluminum foil clip at one end of the isolated fiber. This finger was used to eliminate twisting of the fiber. The aluminum foil clip at the other end of the fiber was hooked by a platinum wire which led through the chamber wall to a tension transducer mounted on the outside of the chamber. The transducer was made with two piezoresistive elements (Pixie 8101, Endevco Lab., Pasadena, Calif.) and had a resolution of ~2 dyn.

Fiber Viability

Several tests of the viability of an isolated fiber were performed. First, the fiber was stimulated electrically with a single pulse of amplitude 5 V and duration 0.5 ms at several points along its length using a pair of platinum wire electrodes. Identical twitch tension traces implied uniform propagation of the action potential. Secondly, the fiber was checked for an all or nothing response. The fiber was placed between two parallel platinum plates (3 mm × 15 mm × 1 mm) mounted 4 mm apart. For undamaged fibers, amplitudes of twitch stimuli less than a threshold value (3–4 V) produced no tension, whereas amplitudes greater than threshold produced the same twitch tension trace.

As a third check on fiber viability, the uniformity of sarcomere length along the fiber was measured at rest and during 200 ms tetani. To effect tetanic stimulation, alternating polarity pulses of 0.5 ms duration and usually 5 V amplitude were applied to the parallel platinum plates. Stimulation frequency was 40 Hz at 6°C, 67 Hz at 11°C, and 100 Hz at 20°C. The sarcomere length was deduced from the position of the first order maximum in the diffraction pattern produced by a 1-mW He-Ne laser beam (model 132, Spectra-Physics Inc., Mountain View, Calif.). The sarcomere lengths near the ends and middle of an undamaged fiber generally differed by <0.05 μm and never differed by >0.1 μm when the resting sarcomere length was 2.1 μm and the contracting sarcomere length was 2.0 μm.

Finally, the fiber was examined at a magnification of 500× using a Zeiss standard microscope equipped with a 40× water immersion objective (N.A. = 0.75) (Carl Zeiss, Inc., New York). A fiber which failed the viability tests exhibited obvious visible damage as well. After successful completion of these tests, the fiber was stored overnight at 4°C. The tests were repeated briefly the next morning.

Before beginning the light-scattering experiments, a fiber was observed at 500× magnification during one or two 2-s tetani. Drift of the fiber through the field of view (300 μm) was <10 μm/s, and motion of one portion of the fiber relative to another was, if discernible at all, <3 μm/s.

After securing the lid, the chamber was filled with Ringer's solution. The entire chamber was then submerged in a constant temperature bath (±0.02°C) which had entrance and exit windows for the incident and scattered light. Filtered Ringer's solution at the bath temperature was continuously circulated through the chamber, except during data collection.

IFS Spectrometer

Fig. 1 is a sketch of the IFS spectrometer and the data collection electronics. The incident beam was the unfocused ($1/e^2$ diam = 2.5 mm) output of an argon ion laser (model 52A, Coherent Radiation, Palo Alto, Calif.). A TEM_{00} single axial mode of the 488-nm line was selected with a prism and an etalon inside the resonant cavity. Less than 1 mW was intercepted by the fiber whose axis was oriented perpendicular to the beam either horizontally or vertically. A prism polarizer rendered the incident electric field vertical, perpendicular to the horizontal scattering plane formed by the incident beam and the light scattered at an angle θ. The detection optics consisted of a front aperture (typically 250 μm diam), an imaging lens which imaged the fiber on the rear slit, a prism analyzer which selected the vertical electric field, a rear slit (typically 240 μm × 1 mm) oriented with the long dimension perpendicular to the fiber axis, and a photomultiplier (F4085, ITT, Fort Wayne, Ind.). The distances from the fiber to the front aperture and from the front aperture to the rear slit were each 20 cm. The front aperture and rear slit were chosen so that the photocathode viewed a portion of the fiber which consisted of the full cross section of the fiber and a length of fiber of ~200 μm. The numerical aperture of the detection optics was sufficiently small so that the photocathode could not resolve the axial separation of two points within the fiber.

The unfocused incident beam and the rear slit were intended to minimize intensity changes in the scattered light due to movement of the fiber. A 150-μm movement of a fiber perpendicular to its axis and the beam resulted in a 25% change in photomultiplier count rate. While a 150-μm movement commonly accompanied the transition from rest to contraction at a sarcomere length of 2.0 to 2.1 μm, no movement perpendicular to the fiber axis was observed at a magnification of 500× during the tetanus tension plateau. Further, an active fiber's position was reproducible to within a few micrometers from tetanus to tetanus. Fiber movement accompanying the transition from rest to contraction was diminished when fibers were stretched beyond 2.1 μm.

Photomultiplier pulses were amplified, discriminated, and then counted by a multiscaler-autocorrelator which transferred its contents to a minicomputer (Nova 2; Data General Corp., Southboro, Mass.) periodically during a tetanus. In the multiscale mode, data consisted of the numbers of counts recorded in 40 contiguous 2-ms time intervals (sample times), then a gap of 20 ms while the multiscaler transferred data to the minicomputer, another record of 40 contiguous 2-ms sample times, another gap

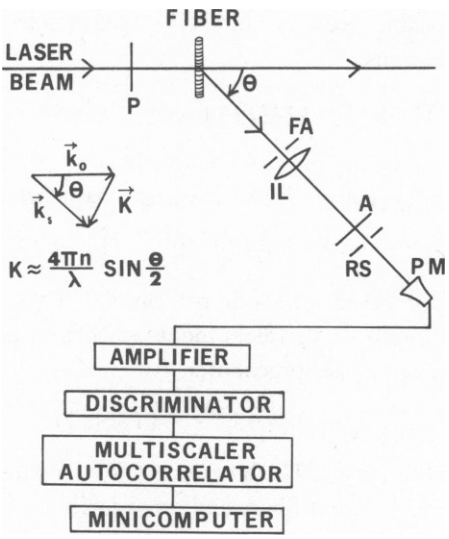

FIGURE 1 IFS spectrometer and data accumulation electronics: (P) polarizer, (FA) front aperture, (IL) imaging lens, (A) analyzer, (RS) rear slit, and (PM) photomultiplier.

of 20 ms, etc., for the duration of the isometric tetanus. After the tetanus, the normalized intensity autocorrelation function $g^{(2)}[\tau]$ and sometimes the photocounting probability density, $P(n)$, were calculated by the minicomputer. $P(n)$ is the probability of recording n counts in a 2-ms sample time. When examining time scales shorter than 2-ms, the autocorrelate mode was used. In this mode the one-bit-scaled intensity autocorrelation function $G_s^{(2)}[\tau]$ was accumulated and transferred to the minicomputer several times during the tetanus. The scaled autocorrelation function is defined by

$$G_s^{(2)}[\tau] = \langle n_s(t)n(t + \tau)\rangle, \qquad \tau \neq 0,$$

where scaled counts n_s are obtained by generating one count for every s^{th} photocount (20, 21). There was no way to calculate $P(n)$ when the autocorrelate mode was used.

Procedure

The tension plateau of a 2.0-s isometric tetanus was reached usually within 0.3 s of the first stimulus, and data were utilized typically between 0.4 and 2.0 s. Fibers were mounted horizontally unless described as mounted vertically, and the scattering angle ranged from 7.5 to 45°. The detection optics were positioned in a minimum of the diffraction pattern unless the detection position is described as a diffraction maximum. The length of the fiber segment viewed by the detection optics was usually $180/\cos\theta$ μm, but was varied from $48/\cos\theta$ to $360/\cos\theta$ μm. Sarcomere length was 2.0 to 2.1 μm, unless described as longer.

Tension was recorded and used as a monitor of fiber viability. Tension plateaus were flat to within 5%. Assuming a circular cross section and using an average measured diameter for each fiber, the tension per cross sectional area ranged from 1.4 to 3.3 Mdyn/cm^2.

Three to six successive 2.0-s tetani were performed for a particular set of parameters. Data from this group of tetani were combined according to a procedure discussed in Appendix A.

RESULTS

Typical Measurement

The upper curve of Fig. 2 is $g^{(2)}[\tau] - 1$ measured during the tension plateau of four successive tetani of a single fiber. The fiber axis was horizontal and the scattering angle was 45°. When τ is much longer than the time scale of intensity fluctuations, $n(t)$ and $n(t + \tau)$ are uncorrelated, and $g^{(2)}[\tau]$ becomes

$$g^{(2)}(\text{long } \tau) = \langle n(t)\rangle \langle n(t + \tau)\rangle / \langle n\rangle^2 = 1.$$

Hence $g^{(2)}(\tau)$ decays from a value of $1 + A$ for short τ to a value of 1 for long τ. To characterize the time dependence of $g^{(2)}[\tau]$ with a single parameter, $\tau_{1/2}$ is defined so that

$$g^{(2)}[\tau_{1/2}] - 1 = \tfrac{1}{2}[g^{(2)}[0] - 1] = A/2.$$

The value of $\tau_{1/2} = 92$ ms observed for the upper curve of Fig. 2 was typical. 18 groups of tetani representing nine different single fibers mounted horizontally and examined at angles of 25 to 45° yielded a mean for the reciprocal of $\tau_{1/2}$ of

$$\langle 1/\tau_{1/2}\rangle = 13.7 \text{ s}^{-1} \text{ (Table I).}$$

An effective $\tau_{1/2}$ was therefore 73 ms. The large standard deviation listed in Table I was due primarily to variation among different fibers and secondarily to the correlation of $1/\tau_{1/2}$ with scattering angle (see Halftime Versus Angle section). These $\tau_{1/2}$ values are roughly 30 times the values found by Bonner and Carlson (10) using whole sartorius muscle (see Discussion section).

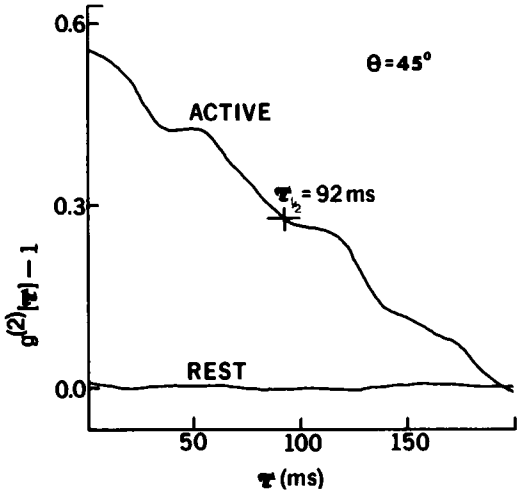

FIGURE 2

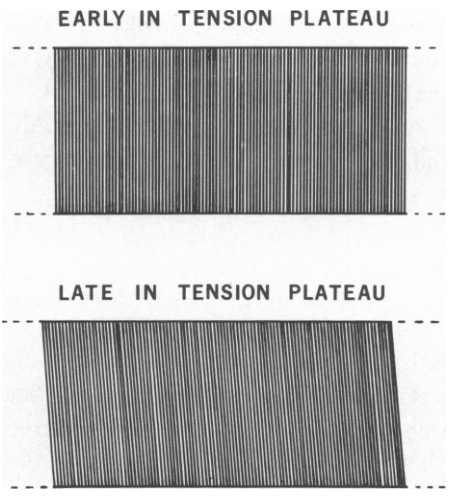

FIGURE 3

FIGURE 2 Active: $g^{(2)}[\tau] - 1$ measured during the tension plateau, 0.4–2.0 s after first stimulus, of four successive tetani. Rest: $g^{(2)}[\tau] - 1$ measured during rest (three successive data batches, each of 1.7-s duration).

FIGURE 3 Sketches of a muscle fiber early and late in the tension plateau of a 2-s tetanus. The scale of the sketches is appropriate for a 100-μm diam fiber and a sarcomere length of 2.0 μm. When the depicted situations are assumed to occur at a time interval of 1.6 s, the rms relative velocity of scattering material is 2.5 μm/s, and the resulting half time of $g^{(2)}[\tau]$ is 38 ms.

Repeated measurements in the autocorrelate mode revealed that $g^{(2)}[\tau]$ was flat on time scales shorter than a few milliseconds. Therefore most data were collected in the multiscale mode, making it possible to calculate the photocounting probability density, $P(n)$.

The value of the amplitude, $A = g^{(2)}[0] - 1 = 0.55$, of the upper curve of Fig. 2, was also typical. 18 groups of tetani involving nine different single fibers mounted horizontally and examined at angles of 25 to 45° yielded a mean amplitude of 0.58 (Table I). The theoretical amplitude expected for Gaussian field statistics is 0.66. The significance of the slight discrepancy is discussed at the end of Appendix A.

A comparison of data taken in different halves of the same tetanus supports the view that the fluctuations in intensity of light scattered from an isometrically contracting fiber arise

TABLE I
STATISTICAL ANALYSIS OF MEASURED PARAMETERS

Parameter	Mean	Standard deviation	Standard deviation of the mean
$\langle A \rangle_{18}$	0.58	± 0.11	± 0.03
$\langle 1/\tau_{1/2} \rangle_{18}$	13.7 s^{-1}	± 7.2 s^{-1}	± 1.7 s^{-1}
$\langle D_I \rangle_{28}$	0.08	± 0.35	± 0.07
$\langle D_A \rangle_{28}$	0.23	± 0.57	± 0.11
$\langle D_r \rangle_{28}$	−0.46	± 0.64	± 0.12
$\langle r \rangle_{18}$	0.25	± 0.14	± 0.03
r_{theor}	0.28		

from a quasi-stationary random process. Measurements of $P(n)$ suggest that the scattered field is Gaussian distributed to a good approximation. The details of these measurements and analyses are presented in Appendix A.

A tetanus plateau contained typically 10–30 half times of $g^{(2)}[\tau]$. The statistical accuracy and bias associated with experiments of such short duration are also discussed in Appendix A.

Resting Muscle

The intensity of light scattered from resting fibers was constant over time intervals of a few minutes. The two curves in Fig. 2 are measurements of $g^{(2)}(\tau)$ performed at $\theta = 45°$ during the active and resting states of the same fiber. 100 measurements of $g^{(2)}(\tau)$ each of 2-s duration yielded an average amplitude <0.01. Background scattering from dust in the Ringer's solution amounted to ~0.5% of the total scattered intensity, and could account for these small intensity fluctuations. However, large fluctuations in the intensity of light scattered from resting fibers were observed over time intervals of 15 to 30 min, and were accompanied by rearrangements of the visible fine structure in the maxima of the diffraction pattern. These slow fluctuations were more rapid immediately after a tetanus.

Halftime Versus Angle

Measurements of $g^{(2)}(\tau)$ were made at various scattering angles, θ, for four single fiber preparations and one bundle of eight fibers. In Fig. 4 the reciprocals of the half times are plotted versus K_F, the projection of the scattering vector on the fiber axis (Fig. 1). For the

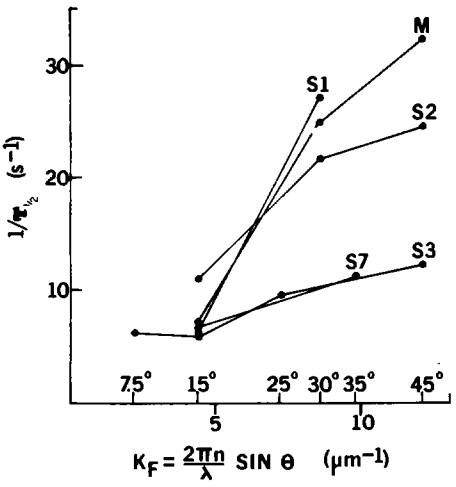

FIGURE 4

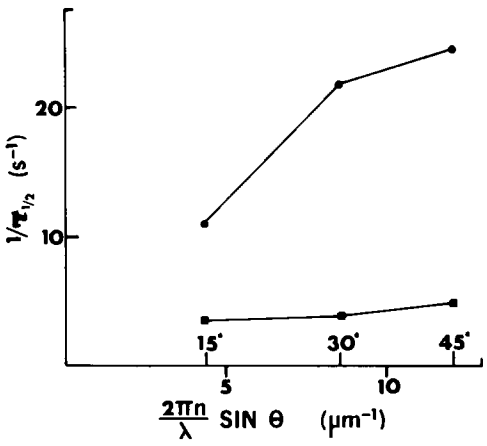

FIGURE 5

FIGURE 4 The reciprocal of the half time of $g^{(2)}[\tau]$ is plotted versus the projection of the scattering vector on the fiber axis. The fiber axis was oriented horizontally. Solid lines connect data points obtained from the same preparation. S1, S2, S3, and S7 were single fiber preparations, and M was a bundle of eight fibers.
FIGURE 5 The reciprocal of the half time of $g^{(2)}[\tau]$ is plotted versus $(2\pi n/\lambda)$ sin θ for the horizontal (circles) and vertical (squares) orientation of the fiber axis of the same preparation (S2). For the horizontal orientation, $K_F = (2\pi n/\lambda)$ sin θ, whereas for the vertical orientation, $K_F \leq 1.5\ \mu m^{-1}$.

usual horizontal orientation of the fiber axis,

$$K_F = (2\pi n/\lambda) \sin \theta.$$

While considerable variation existed between different preparations, there was a roughly linear relation between $1/\tau_{1/2}$ and K_F for a given preparation. Measurements of $g^{(2)}(\tau)$ were made on one fiber (S2) whose axis was oriented first horizontally and then vertically. In the latter situation, the direction of the fiber axis deviated a few degrees from vertical so that the detection optics sampled an area of the diffraction pattern just off the zero order maximum. In Fig. 5 $1/\tau_{1/2}$ is plotted versus $(2\pi n/\lambda) \sin \theta$ for both the horizontal and vertical orientations of the fiber axis. The half times measured when the fiber axis was oriented vertically were long enough to be severely biased (Appendix B). The value of K_F was $\leq 1.5\ \mu m^{-1}$ when the fiber axis was oriented nearly vertically.

The roughly linear relation between $1/\tau_{1/2}$ and K_F evident in Fig. 4 for a given preparation is consistent with a model of a fiber in which scattering material possesses relative velocities which are constant for time intervals longer than the field coherence time. That $1/\tau_{1/2}$ was substantially reduced for small values of K_F implies that polarizability fluctuations, whose effect on $g^{(2)}[\tau]$ would be independent of K_F, did not contribute strongly to the observed decay of $g^{(2)}[\tau]$ at $\theta = 25$ to 45°. The small values of $1/\tau_{1/2}$ measured when the fiber axis was oriented vertically imply that relative velocities of scattering material were directed primarily along the fiber axis.

Appendix C outlines the calculation of $g^{(2)}[\tau]$ for a model situation in which many identical Rayleigh scatterers are positioned randomly throughout a cylindrical scattering volume (e.g., a segment of a muscle fiber). The scatterers possess constant velocities along the cylinder axis such that the tilting effect depicted in Fig. 3 is obtained. The rms relative velocity, σ_v, is rather insensitive to the shape of the cross section of the cylinder, and satisfies the relation

$$\sigma_v = 0.81/K_z\tau_{1/2}.$$

For a $\tau_{1/2}$ of 70 ms at $\theta = 30°$, $\sigma_v = 1.3\ \mu m/s$.

Halftime Versus Length of Fiber Viewed

Five of the ten fibers used in these experiments exhibited a slow elongation (<1%/s) of the sarcomeres near the middle of the fiber during the tetanus plateau, even at sarcomere lengths of 2.0 to 2.1 μm. The elongation was detected by a slow movement of the position of the first order maximum in the diffraction pattern. Three of these five fibers exhibited movement of the diffraction maxima only after 20–30 2-s tetani had been performed. The presence of movement of the first order maximum correlated well with shorter values of $\tau_{1/2}$ (40–70 ms) for $\theta = 25$ to 45°, while the absence of movement correlated well with longer values of $\tau_{1/2}$ (70–100 ms). The extent to which measurements of $g^{(2)}(\tau)$ reflect relative motion accompanying slow elongation of fibers was investigated experimentally.

Measurements of $g^{(2)}(\tau)$ were performed on one fiber (S3) while the length of the fiber viewed by the detection optics was varied by altering the dimensions of the front aperture and rear slit. Fiber S3 was one of five fibers which exhibited no visible movement of the diffraction maxima. Using the standard detection optics, the measured $\tau_{1/2}$ for this fiber was 82 ms at $\theta = 45°$. In Fig. 6 $1/\tau_{1/2}$ is plotted versus the width of the rear slit, which is roughly

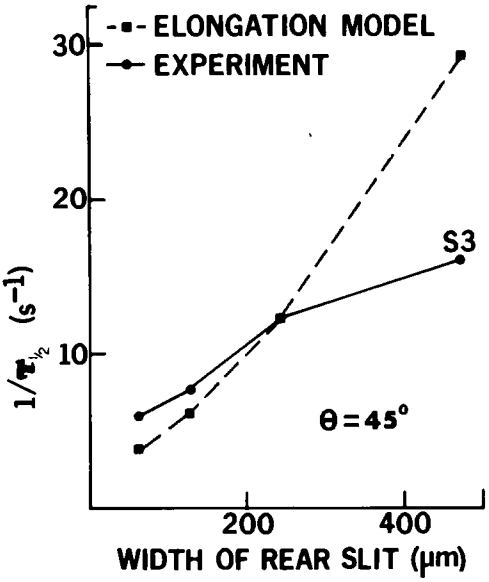

FIGURE 6 The reciprocal of the half time of $g^{(2)}[\tau]$ was measured with four different configurations of the detection optics. The diameter of the front aperture and the width of the rear slit were, respectively: 1 mm × 63 μm, 500 μm × 125 μm, 250 μm × 240 μm, 100 μm × 470 μm. The squares indicate values of $1/\tau_{1/2}$ calculated from the elongation model of Appendix D. An elongation rate of 0.5%/s was used to match the $\tau_{1/2}$ of 82 ms measured at a slit width of 240 μm.

proportional to the length of the fiber viewed by the detection optics. $1/\tau_{1/2}$ increased by a factor of 2.7 when the width of the rear slit increased by a factor of 7.5.

If the only relative motion of scattering material within a fiber is the relative motion accompanying slow elongation of a fiber, then the relation between $1/\tau_{1/2}$ and the width of the rear slit can be calculated theoretically. Appendix D outlines the calculation of $g^{(2)}(\tau)$ for a model situation in which scatterers are positioned randomly throughout the scattering volume, and the velocities of the scatterers are such that the ensemble of scatterers possesses a constant rate of elongation along an axis (e.g., the fiber axis). The values of $1/\tau_{1/2}$ predicted for this model situation are plotted in Fig. 6 for the four different configurations of the detection optics. If elongation of fiber S3 occurred but was too slow to result in visible movement of the diffraction maxima, and if the relative motion accompanying elongation was the only relative motion which occurred during the tetanus plateau, the measured $1/\tau_{1/2}$ should have increased by a factor of 9.6 when the width of the rear slit increased by a factor of 7.5. Hence, while relative motion associated with fiber elongation may have contributed to the decay of $g^{(2)}(\tau)$, it was not the dominant contribution when no visible movement of diffraction maxima was observed.

Note that a small fraction of the increase in $1/\tau_{1/2}$ observed when the scattering angle was increased (Fig. 4) was due to the increase in the length of fiber viewed by the detection optics ($180/\cos\theta$ μm). For fiber S3 an increase in θ from 7.5 to 45° corresponds to an increase of 40% in the length of fiber viewed, which implies an increase in $1/\tau_{1/2}$ of 15% (deduced from Fig. 6) as compared with the factor of 2 increase observed (Fig. 4).

Amplitude Versus Angle

Relative axial displacements of scattering material which are constrained to values $<1/K_F$ result in values for the amplitude of $g^{(2)}[\tau]$ which are reduced from the values resulting from unconstrained motion. An estimate of the reduction in amplitude can be obtained by considering a model situation in which many independent, identical, Rayleigh scatterers are randomly distributed throughout the scattering volume. Further, let each scatterer execute motion along the z axis (e.g., the fiber axis) such that displacements about its mean position are constrained by a linear restoring force to an rms value of σ_D. $g^{(2)}[\tau]$ for such a model is derived in the appendix of reference 23, and the result appears as Eq. 12 of the appendix of reference 23. Note that a correction to this equation published later as a letter to the editor (24) replaces γ by $(\gamma/2)$. If the notation change, $q \rightarrow K_z$, is made, and if σ_D^2 is identified with D/γ, the amplitude of $g^{(2)}[\tau]$ can be written $A = g^{(2)}[0] - 1 = 1 - \exp[-2K_z^2\sigma_D^2]$. Taking the amplitude which results from unconstrained motion to be $A = 0.66$, the expected amplitudes for motion constrained to varying extents at various scattering angles are given in Table II. Fig. 7 presents the measured amplitudes of $g^{(2)}[\tau]$ at various scattering angles for four single fiber preparations and one bundle of eight fibers. Measured values of $1/\tau_{1/2}$ plotted versus K_F for these same preparations are presented in Fig. 4. The plots of amplitude versus K_F are somewhat variable. Preparations M, S1, and S2 exhibited slow elongation (1%/s) of the central portion of the fiber during the tension plateau, and yielded larger values of $1/\tau_{1/2}$. If the amplitudes for these three preparations are averaged, the average amplitude at $\theta = 15°$ is 90% of the average amplitude at $\theta = 30°$. Since the value of $\tau_{1/2}$ at $\theta = 15°$ was about twice the value at $\theta = 30°$ for these preparations, the statistical bias (Appendix B) was more severe at $\theta = 15°$ than at $\theta = 30°$ and could account for the 10% reduction in amplitude. Preparations S3 and S7 exhibited no visible movement of the diffraction maxima, and, as discussed previously, fiber S3 exhibited an elongation rate <0.5%/s. Fiber S7 exhibited an amplitude at $\theta = 15°$ slightly greater than the value at $\theta = 35°$. However, fiber S3 exhibited an amplitude at $\theta = 7.5°$ which was 35% of the average of the amplitudes at $\theta = 25°$ and $\theta = 45°$. The more severe bias at $\theta = 7.5°$ could account for a 15% reduction in amplitude, leaving a 50% reduction unaccounted for. Because of the variability of the data the possibility cannot be rigorously excluded that the motion responsible for the decay of $g^{(2)}[\tau]$ in fibers exhibiting no elongation is constrained to rms relative displacements as small as 0.3 μm.

TABLE II
AMPLITUDE OF $g^{(2)}[\tau]$ RESULTING FROM MOTION CONSTRAINED TO AN RMS DISPLACEMENT OF σ_D FOR VARIOUS SCATTERING ANGLES

RMS Displacement	$A = g^{(2)}[0] - 1 = 0.66\{1 - \exp[-2K_z^2\sigma_D^2]\}$		
σ_D	$\theta = 7.5°$	$\theta = 15°$	$\theta = 30°$
(micrometers)			
0.01	0.001	0.003	0.01
0.05	0.02	0.06	0.20
0.10	0.06	0.22	0.51
0.20	0.22	0.52	0.66
0.30	0.39	0.64	0.66
observed	>0.25	>0.30	0.58

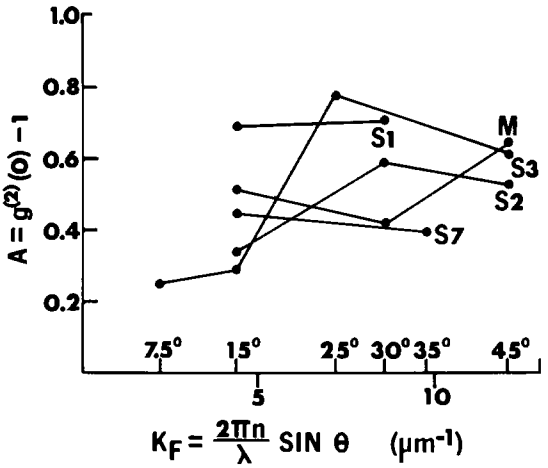

FIGURE 7 The measured amplitude is plotted versus the projection of the scattering vector on the fiber axis for four single fiber preparations and one bundle of eight fibers. The fiber axis was oriented horizontally. Solid lines connect data points from the same preparation.

Diffraction Maxima

Measurements of $g^{(2)}[\tau]$ were made on the first order maximum of the diffraction pattern. Since the diffraction maxima are comprised predominantly of elastically scattered light, small amplitudes were expected. Measurements of $g^{(2)}[\tau]$ in a diffraction minimum (θ = 35°) and on the first order maximum (θ = 10.6°) were performed on fiber S8 and are presented in Fig. 8. If the fine structure or speckle of the first order maximum swept across the front aperture during a tetanus plateau, $g^{(2)}[\tau]$ could not be measured reliably on the diffraction maximum.

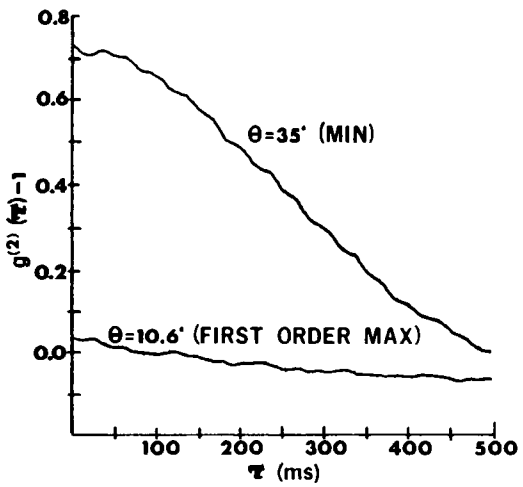

FIGURE 8 Measurements of $g^{(2)}[\tau]$ were made on the first order diffraction maximum (θ = 10.6°; data taken during the tension plateau, 0.5–2.0 s after first stimulus, of four successive tetani) and in a diffraction minimum (θ = 35°; data taken during the tension plateau, 0.5–2.0 s after first stimulus, of four successive tetani) for fiber S8.

Accordingly, the sarcomere length had to be constant to better than 0.5%/s. Fiber S8 exhibited no visible movement of the diffraction maxima, and the half time measured at $\theta = 35°$ was 264 ms. The amplitude measured on the first order maximum was approximately $A = 0.03$. Similar results were obtained on the zero order maximum (fiber axis oriented vertically and $\theta = 3°$).

Halftime Versus Sarcomere Length

Measurements of $g^{(2)}[\tau]$ were performed on fiber S6 at sarcomere lengths of (in chronological order) 2.05, 2.80, 3.40, 4.00, and 2.30 μm. The sarcomere length was inferred from the position of the first order diffraction maximum. The tension traces are reproduced in the lower half of Fig. 9. The traces at longer sarcomere lengths exhibited the tension creep phase described previously by Gordan et al. (7). The creep phase was accompanied by elongation (5–10%) of the illuminated sarcomeres which were near the middle of the fiber, as evidenced by the movement of the first order diffraction maximum. The tension trace at $S = 4.00$ μm showed significant tension development. Note, however, that only the sarcomeres near the middle of the fiber were known to be stretched beyond overlap of thick and thin filaments. Further, only the tension creep phase was evident in the tension trace; there was no fast tension rise upon stimulation. Upon returning from no overlap conditions, the tension trace at $S = 2.30$ μm was similar to the trace at $S = 2.05$ μm, but was reduced to 85 dyn. Half times were calculated for the period of the tetanus, 0.9–2.0 s, which was contained in the period of tension plateau for all sarcomere lengths, and for the period, 0.5–1.2 s, which contained

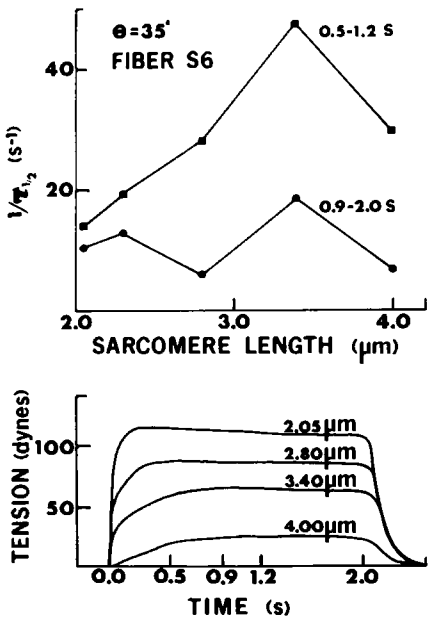

FIGURE 9 Lower half: tension traces from fiber S6 at four different sarcomere lengths. Upper half: the reciprocal of the half times during the tension plateau (circles) and during the tension creep phase (squares).

portions of the tension creep phase at longer sarcomere lengths. The reciprocals of the half times for these two periods at five sarcomere lengths are plotted in the upper half of Fig. 9. Both the amplitude and the decay rate $1/\tau_{1/2}$ of $g^{(2)}[\tau]$ during the tension plateau were roughly independent of sarcomere length. The elongation of the middle of the fiber during the tension creep phase resulted in a significantly greater decay rate than during the tension plateau.

DISCUSSION

Previous Work

Bonner and Carlson (10) reported half times for the decay of $g^{(2)}[\tau]$ of 2–3 ms at $\theta = 30°$ during isometric contraction of frog sartorius muscle at rest length. The half times reported by Bonner and Carlson for whole muscle preparations are therefore a factor of 30 faster than the half times reported here for single fiber preparations ($\tau_{1/2} = 70$ ms). One would expect interfiber motion in a multifiber preparation to result in half times faster than those observed with single fiber preparations. However, not all of the discrepancies between the results reported by Bonner and Carlson and the single fiber results reported here can be explained by the possible presence of interfiber motion. For example, Bonner and Carlson reported half times of 4 ms for small bundles of fibers from the semitendinosus muscle at sarcomere lengths of 2.8–3.1 μm, while half times of 40 ms are reported here for an eight fiber bundle at rest length. It seems unlikely that the difference in sarcomere lengths could account for the factor of 10 difference in half times.

Fujime et al. (25) have reported measurements of $g^{(2)}[\tau]$ during isometric contraction of frog sartorius muscle which corroborate the measurements reported by Bonner and Carlson (10). However, when Fujime et al. (25) used frog sartorius muscles <1 mm thick, the amplitude of $g^{(2)}[\tau]$ measured on the zero order maximum was ~ 0. Similar results were obtained by Fujime et al. (25) when bundles of glycerinated or skinned rabbit psoas fibers were used under conditions in which the preparation developed low tension (low temperature and/or low calcium ion concentration). The low amplitude measured on the zero order maximum by Fujime et al. differs from the results reported by Bonner and Carlson (10), but agrees with measurements reported here (see Diffraction Maxima section).

In view of these discrepancies, two points deserve mention. First, muscle preparations which are thicker than 1 mm constitute a deep phase screen and are difficult to view reliably under the microscope. Interfiber motion during isometric contraction is therefore difficult to monitor and can result in random phase modulation of the transmitted and scattered light. If interfiber motion occurs in a thick preparation, the measured $g^{(2)}[\tau]$ can decay artefactually fast and can be roughly independent of the scattering angle, resulting in nonzero amplitudes on the diffraction maxima. Second, interfiber motion in thin muscle preparations can lead to artefactually fast decays of $g^{(2)}[\tau]$, although low amplitudes should be measured on the zero order maximum. (Twisting of the preparation, however, can lead to nonzero amplitudes on the zero order maximum, except for very small scattering angles.) The viable, intact, single fiber exhibits good structural integrity during isometric contraction, can be reliably monitored through the microscope for gross relative motion, and hence should be the most reliable preparation for these light-scattering techniques.

Possible Artefacts

Two possible sources of artefact deserve mention. While $g^{(2)}[\tau]$ is insensitive in principle to a drift velocity of a fiber through the scattering volume, the introduction of a new portion of fiber into the scattering volume will result in a new speckle pattern and an intensity change at the cathode of the photomultiplier. The time scale of these intensity fluctuations will be equal to the time required for a significant fraction of the scattering volume to be occupied by a new portion of fiber. The drift velocities observed through the microscope (500×) were always <10 μm/s, so that 10% of the 200-μm long scattering volume would be replaced by a new portion of fiber in a time not <2 s. This minimum estimate of the time scale is a factor of 20 to 40 longer than the time scale of the observed intensity fluctuations.

The possibility of transverse or longitudinal oscillations of a fiber during isometric contraction deserves consideration. The period of the fundamental transverse oscillation for a 100-μm diam fiber is given by $2[ML/T]^{1/2}$, where M and L are the mass and length of the fiber, and T is the tension developed by the fiber (26). The period of the fundamental longitudinal oscillation is given by $2[MC]^{1/2}$, where C is the compliance of the active fiber (19, 26). Using $M = 8 \times 10^{-5}$ gm, $L = 1.0$ cm, $T = 200$ dyn, and $C = 2 \times 10^{-5}$ cm/dyn, the periods of transverse and longitudinal oscillation are ~1 and 0.1 ms, respectively. Moreover, these oscillations should be quickly damped (19). It is unlikely that these oscillations contribute to the observed slow decay of $g^{(2)}[\tau]$. It is interesting to note that longitudinal oscillations observed in frog skeletal muscle fibers by Armstrong et al (27) had a period of 30 to 50 ms at 3°C, but it is unlikely that these oscillations could be excited persistently throughout a 2-s tetanus.

Summary

The results of measurements of $g^{(2)}[\tau]$ reported here prompt the following description of a 200-μm segment of a muscle fiber during the tension plateau of an isometric tetanus. No significant fraction of the scattering material possesses relative velocities >3 μm/s accompanied by displacements >0.05 μm. For example, if 100% of the scattering material possessed relative velocities with an rms value of 10 μm/s accompanied by relative displacements with an rms value of 0.05 μm, the observed decay of $g^{(2)}[\tau]$ at $\theta = 30°$ would have included a fast component ($\tau_{1/2} = 10$ ms) with a contribution to the amplitude of 0.2. No such fast component was observed. The observed variation of the decay rate ($1/\tau_{1/2}$) with scattering angle and orientation of the fiber axis implies that the decay of $g^{(2)}[\tau]$ was due primarily to relative motion of the scattering material along the fiber axis. An rms value for these relative axial velocities was 1–2 μm/s. The large amplitudes of $g^{(2)}[\tau]$ observed at $\theta = 7.5°$ to $\theta = 30°$ (Table II) exclude the possibility that the motion responsible for the observed decay of $g^{(2)}[\tau]$ was constrained to relative displacements with an rms value ≤0.1 μm. The measurements of amplitude versus scattering angle are not sufficiently reliable to exclude the possibility that the relative motion responsible for the decay of $g^{(2)}[\tau]$, particularly in those fibers exhibiting minimal gross motion, was constrained to relative displacements with an rms value as small as 0.3 μm. Note that the possibility of relative motion constrained to 0.3 μm is not in conflict with the roughly linear relation observed between $1/\tau_{1/2}$ and K_F. Velocities of scattering material which are constant for time periods greater than the coherence time result in a linear relation between $1/\tau_{1/2}$ and K_F. The measured $\tau_{1/2}$ of 70 ms at $\theta = 30°$ corresponds to an rms relative

velocity of 1.3 μm/s and a τ_{COH} of ~200 ms. Velocities constant over τ_{COH} would result in relative displacements of 0.3 μm.

Repeated observations through the microscope (500×) of fibers in isometric contraction revealed axial translation of one portion of a fiber relative to another with relative velocities in the range 1–2 μm/s (Fig. 3). The light-scattering results are entirely consistent with this large scale relative motion (many myofibrillar sarcomeres moving in concert relative to other large groups of sarcomeres).

The light-scattering data does not exclude structural fluctuations on the scale of the myofibrillar sarcomere arising from force imbalances due to independent cross-bridge cycling. However, an upper limit of 3 μm/s may be placed on relative axial velocities of thick or thin filaments involving relative axial displacements >0.05 μm. Further, if such small scale structural fluctuations contributed significantly to the observed decay of $g^{(2)}[\tau]$, a significant change in the amplitude and decay rate of $g^{(2)}[\tau]$ would be expected at no overlap conditions. Both the amplitude and $1/\tau_{1/2}$ were roughly independent of sarcomere length.

It is worth noting several possible explanations for the lack of evidence in the present measurements for structural fluctuations on the scale of the myofibrillar sarcomere. First, of course, the current model of asynchronously cycling cross-bridges may not be correct. Second, the structural rigidity of *M* and *Z* lines may be sufficient to constrain thick and thin filaments to relative displacements <0.05 μm. Third, during isometric contraction, cross-bridges may be attached to the thin filaments for a large fraction of the cross-bridge cycle, thereby conferring sufficient structural rigidity to render relative displacements unresolvable. Finally, the upper limit set by the present results for the relative velocities involved in such structural fluctuations (3 μm/s) corresponds to the relative velocity of thick and thin filaments during unloaded shortening of a fiber. Relative velocities of thick or thin filaments <1–2 μm/s would be masked by the large scale relative motion.

This work was supported by U.S. Public Health Service/National Institutes of Health grant AM12803 awarded to Dr. Carlson, and Muscular Dystrophy Association postdoctoral fellowships awarded to Dr. Haskell.

APPENDIX A

Stationarity, Statistical Accuracy and Bias, Method for Combining Data, and Field Statistics

STATIONARITY The analysis and discussion of $g^{(2)}[\tau]$ presented in this paper implicitly assumes that the scattered intensity during the tension plateau of an isometric tetanus is a random variable associated with a stationary, or at least quasi-stationary, random process. This assumption was investigated experimentally.

The mean intensity $\langle I \rangle$, the amplitude $A = g^{(2)}[0] - 1$, and the half time $\tau_{1/2}$ were examined for systematic variation during the tension plateau. Values for these three parameters were calculated for the first and second halves of the tension plateaus of 28 groups of tetani involving 10 different fibers which were mounted horizontally and examined at angles of 7.5 to 45°. The parameter D_I was defined to be

$$D_I = 2[\langle I \rangle_{FH} - \langle I \rangle_{SH}] / [\langle I \rangle_{FH} + \langle I \rangle_{SH}],$$

where the subscripts FH and SH denote first half and second half, respectively. The average of D_I over the 28 groups of tetani was computed. Similar analyses were performed for the amplitude and half time. For a stationary process the mean values of D_I, D_A, and D_τ should be zero.

Table I lists the results of the calculations. In proceeding from the first to the second half of the tension plateau, the mean intensity was nearly the same, while the amplitude decreased by 23% and the half time increased by 46%. Evidently the intensity fluctuations are due to a random process which is only quasi-stationary, and care must be taken to compare equivalent portions of the tension plateau when varying other parameters.

STATISTICAL ACCURACY Since the average number of photocounts in a coherence time of the scattered field was very much larger than one, the statistical accuracy of $g^{(2)}[\tau]$ in the muscle measurements was limited by the number of coherence times contained in the duration of the tension plateau (22). The effect of shot noise was negligible. The statistical accuracy of $g^{(2)}[\tau]$ in the muscle measurements can be estimated by performing a rigorous calculation for a model situation which approximates the muscle conditions. Appendix B describes such a model situation, and outlines the calculation of the statistical accuracy of $g^{(2)}[\tau]$. The relative error of $g^{(2)}[\tau] - 1$ for small τ was found to be 0.30 for a 4.8-s measurement. From these results the relative error of the amplitude for a group of three tetani can be expected to be 0.30. The observed relative error is the ratio of the standard deviation to the mean of the amplitude quoted in Table I, or $0.11/0.58 = 0.19$.

BIAS As a result of the relatively few coherence times contained in the duration of a tension plateau, the statistical bias of $g^{(2)}[\tau]$ was significant. The magnitude of the bias for the muscle measurements can be estimated by considering the model calculations outlined in Appendix B. On the basis of the results presented in Appendix B, the measured amplitude for a group of three tetani can be expected to underestimate the true amplitude by 9%. Moreover, a measured half time of 70 ms corresponds to a true half time of 75 ms. For a single tetanus the measured amplitude underestimates the true amplitude by 27% and a measured half time of 59 ms corresponds to a true half time of 75 ms.

COMBINING DATA There are two obvious ways to combine data from the three to six successive tetani which comprise a group. The first method consists of averaging the individual $g^{(2)}[\tau]$. If this method is used, the statistical accuracy of a group of three 1.6-s tetanus plateaus is equivalent to that of one 4.8-s plateau. However, the bias of the group amplitude and half time derived with this first method is the bias associated with a 1.6-s measurement, roughly 20–30% (see Appendix B and the previous Bias section).

A second method consists of averaging the individual $G^{(2)}[\tau]$ and normalizing by the group average counts per sample time. Using this method, the statistical accuracy of a group of three 1.6-s plateaus is equivalent to that of one 4.8-s plateau, and the bias of the group amplitude and half time is slightly less than the bias associated with a 4.8-s measurement, roughly 7–9% (see Appendix B and the previous Bias section). This second method of combining muscle data, however, assumes that intensity fluctuations in successive tetani arise from a single stationary random process with the same mean intensity. This assumption can be checked experimentally.

The total counts per tetanus plateau, n_P, fluctuates from one tetanus to the next within a group of successive tetani. The ratio of the standard deviation to the mean, $r = \sigma_P / \langle n_P \rangle$, can be calculated theoretically for a stationary random process and compared with the observed value. The mean and standard deviation of the total counts per tetanus plateau were computed for 18 groups of tetani representing nine different fibers mounted horizontally and examined at angles of 25 to 45°. The ratio r was calculated for each group, and the average over the 18 groups was $\langle r \rangle = 0.25$ (Table I). Appendix B outlines the calculation of the expected value of r, assuming a single stationary random process for the several 1.6-s tension plateaus comprising a group of tetani. This theoretical value, listed in Table I, is 0.28.

The observed variation of the total counts per tetanus plateau is roughly the amount to be expected for a single stationary random process. Hence the second method of combining data from tetani within a group seems justified and offers the advantage of reducing the bias of $g^{(2)}[\tau]$. The extent to which the bias is reduced can of course be evaluated by employing both methods of combining data, and comparing the amplitudes and half times derived by the two methods. The observed difference between the two sets of values can be compared with the difference predicted theoretically for the model situation of Appendix B.

Values for the amplitudes and half times were derived by the two methods for 18 groups of tetani representing nine different fibers mounted horizontally and examined at angles of 25 to 45°. It was

found that the amplitude derived by the first method (averaging $g^{(2)}[\tau]$) was on the average 12% less than the mean of the amplitudes derived by the two methods. For the model situation treated in Appendix B, one would expect the amplitude derived by the first method to be 22% less than the mean of the amplitudes derived by the two methods. Similarly, it was found that the half time derived by the first method was on the average 13% less than the mean of the half times derived by the two methods. For the model situation of Appendix B, one would expect the half time derived by the first method to be 17% less than the mean of the half times derived by the two methods. Hence the existence of the biasing effect was verified, though the magnitude of the bias was less than that predicted for the model situation of Appendix B. Unless otherwise specified, all values quoted for group amplitudes and half times have been derived using the second method: averaging the $g^{(2)}[\tau]$ and then normalizing by the group average counts per sample time.

PHOTOCOUNTING PROBABILITY DENSITY The relation between the field and intensity autocorrelation functions, $g^{(2)}[\tau] = 1 + |g^{(1)}[\tau]|^2$, is derived with the assumption of Gaussian field statistics. To check the validity of this assumption in the case of the muscle measurements, the photocounting probability density, $P(n)$, was measured during the tension plateaus of isometric tetani. $P(n)$ is the probability of recording n counts in a 2-ms sample time. $P(n)$ measured during four successive tetani is plotted with a solid line in Fig. 3. $g^{(2)}(\tau) - 1$ measured during these same tetani appears as the upper curve in Fig. 2.

For the case of Gaussian field statistics, a point detector, sample times shorter than the field coherence time, and experiment durations $\geq 500\ \tau_{COH}$, $P(n)$ is simply the Bose-Einstein distribution, and the amplitude $A \simeq \mathrm{Var}(n)/\langle n \rangle^2 \simeq 1.0$. However, if the detector subtends an area which is an appreciable fraction of a coherence area, or if experiment durations are only 20–30 τ_{COH}, $P(n)$ is altered significantly. A calibration scheme was devised which made possible the measurement of the $P(n)$ arising from a scattered field known to be Gaussian distributed, and which took into account not only the spatial averaging effect of the detection optics employed in the muscle measurements, but also the statistical bias accompanying the short experiment durations. The scheme involved the substitution for the muscle fiber of a solution of 0.1-μm diam polystyrene latex spheres (Dow Diagnostics, Dow Chemical Co., Indianapolis, Ind.) in ethylene glycol (viscosity 19.9 cp). In this calibration solution there are many independent spheres contained in any scattering volume which can be defined by the detection optics of the spectrometer. According to the central limit theorem, the field statistics are therefore Gaussian. This point was verified experimentally by observing that the measured amplitude approached 1.0 as the area subtended by the detector approached a small fraction of a coherence area. Next, the calibration scheme involved the focusing of the incident beam to a $1/e^2$ diam of 55 μm in order to simulate the spatial extent of the muscle fiber. Finally, using the detection optics and the data collection format employed in the muscle measurements, $P(n)$ and $g^{(2)}(\tau)$ were measured. At $\theta = 16°$ the time dependence of $g^{(2)}(\tau)$ was exponential with a half time of 75 ms. The $P(n)$ measured in four 1.6-s experiments at a scattering angle of 16° is plotted with a dotted line in Fig. 3.

If the spatial extent of the fiber is properly simulated by the focused beam, and if the electric field scattered from the fiber is Gaussian distributed, the two histograms in Fig. 3 should superpose. The agreement is well within the statistical accuracy of these particular measurements of $P(n)$. However, the average value for the amplitude in the muscle measurements, $A = 0.58$ (Table I), is somewhat lower than the theoretically calculated and experimentally measured average value for the amplitude using the polystyrene latex sphere solution, $A = 0.66$, which includes the effect of the statistical bias of the short experiment duration. This discrepancy in average amplitudes is probably statistically significant, and may indicate the presence in the muscle measurements of a slightly greater statistical bias than reckoned here, or the presence of a small amount of temporally incoherent light in the light scattered from a fiber, perhaps a few percent of the total scattered intensity. While a small amount of elastically scattered light (partial heterodyning) in the muscle measurements could lead to a reduction in amplitude, the $P(n)$ observed deviated from the $P(n)$ calculated assuming Gaussian field statistics in a way which was inconsistent with this possibility. In summary, the electric field scattered from a muscle fiber is Gaussian distributed to a good approximation, and the relation $g^{(2)}(\tau) = 1 + |g^{(1)}(\tau)|^2$ is similarly a good approximation.

APPENDIX B

Calculations Concerning Statistical Accuracy and Bias

Consider a model situation in which the field statistics are Gaussian, the detector subtends an area smaller than a coherence area, and the sample time (2 ms, as in the case of the muscle measurements) is smaller than the field coherence time. The amplitude of $g^{(2)}[\tau]$ in this case is $A = 1.0$. Further, assume that the time dependence of $g^{(2)}[\tau]$ is exponential with a half time of 75 ms. The corresponding field coherence time is 216 ms (see the Introduction–Technique section). Finally, it is assumed that the count rate is sufficiently high that the average number of counts registered per sample time is $\langle n \rangle \geq 50$. See Saleh (22) for a complete discussion of concepts employed in this appendix.

If many statistically independent measurements of $g^{(2)}[\tau]$ are made, each measurement corresponding to an experiment of duration N_{COH} coherence times, the mean and standard deviation of $g^{(2)}[\tau]$ can be experimentally determined. These values can be calculated theoretically for the model situation under consideration. The ratio of the standard deviation of $g^{(2)}[\tau]$ to the mean of $g^{(2)}[\tau] - 1$ for small τ can be shown to be (Eqs. 7.92 and 7.93 of reference 22)

$$\sigma_g/[g^{(2)}[\tau] - 1] = [2/N_{COH}]^{1/2}, \tau \ll \tau_{1/2}.$$

An experiment duration of 4.8 s contains $4.8/0.216 = 22.2$ coherence times and yields a value for the ratio $\sigma_g/[g^{(2)}[\tau] - 1]$ of 0.30.

The finite duration of a measurement of $g^{(2)}[\tau]$ results in a statistical bias of $g^{(2)}[\tau]$, which for the model situation under consideration can be shown to be (an evaluation of the equation at the top of page 382 of reference 22)

$$\text{Bias}[g^{(2)}[\tau]] = -g^{(2)}[\tau]/N_{COH}.$$

Hence the measured amplitude underestimates the true amplitude, $A = 1.0$, according to

$$A_{exp} = 1 - 2/N_{COH}.$$

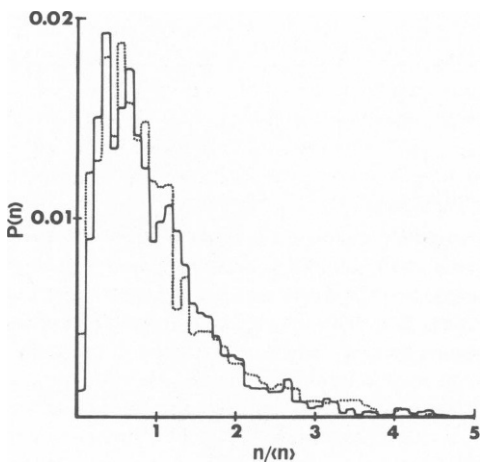

FIGURE 10 Solid line: $P(n)$ measured during the tension plateau, 0.4–2.0 s after the first stimulus, of four successive tetani (group average counts per sample time was 47.9 and $A = 0.55$). Dotted line: $P(n)$ measured using solution of 0.1 μm diam spheres and focused beam (four successive data batches, each of 1.6 s duration; group average counts per sample time was 45.8 and $A = 0.59$).

Using the definition of the half time, the measured half time can be shown to underestimate the true half time $\tau_{1/2}$ according to

$$\tau_{1/2\text{exp}} = \tau_{1/2} \ln [2 - 2/N_{\text{COH}}]/\ln 2.$$

For the model situation under consideration an experiment duration of 4.8 s results in a measured half time of 70 ms and a measured amplitude of 0.91. For models with true half times of 100, 200, and 300 ms, the measured half times are 91, 163, and 208 ms, respectively, and the measured amplitudes are 0.88, 0.76, and 0.64, respectively. Hence for experiment durations of 4.8 s, measured half times >200 ms are quite severely biased.

The variance of the total number of counts registered in an experiment can be calculated theoretically for the model situation under consideration and shown to be

$$\text{Var}[n_P] = \langle n_P \rangle^2 / N_t N_s + \langle n_P \rangle,$$

where $\langle n_P \rangle$ is the mean total counts per experiment, and N_t and N_s are the numbers of independent temporal and spatial modes, respectively (see pages 195–196 of reference 22). N_t and N_s are quantitative measures of the temporal and spatial averaging performed by the detection system. For an experiment of duration 1.6 s, N_t is approximately $N_{\text{COH}} = 1.6/0.216 = 7.4$. For the detection optics of the model situation under consideration, $N_s = 1$. Since $\langle n_P \rangle \geq (1.6 \text{ s}/2 \text{ ms})\ (50) = 40{,}000$, the second term (the shot noise term) in the expression for $\text{Var}[n_P]$ can be neglected so that

$$\text{Var}[n_P] = \langle n_P \rangle^2 / N_t N_s = \langle n_P \rangle^2 / 7.4.$$

The ratio of the standard deviation to the mean of the total counts per experiment is therefore

$$r = \sigma_P / \langle n_P \rangle = [N_t N_s]^{-1/2} = [7.4]^{-1/2} = 0.37.$$

The effect of the detection optics actually employed in the muscle measurements can be taken into account by substituting $N_s = 1/A$, where A is the amplitude listed in Table I. The value of r to be expected is therefore

$$r = [N_t N_s]^{-1/2} = [0.58/7.4]^{-1/2} = 0.28.$$

APPENDIX C

Model Calculation of $g^{(2)}[\tau]$: Tilt Model

Consider a model situation in which there are a large number, N, of identical Rayleigh scatterers positioned randomly throughout a cylindrical scattering volume (e.g., a segment of a muscle fiber). The scatterers possess constant velocities along the cylinder axis (z axis) which is perpendicular to the incident beam (traveling in the positive y direction) and contained in the scattering plane (y-z plane). Let the velocity of the n^{th} scatterer be given by

$$\mathbf{v}_n = v_n \hat{k} = \left(\frac{dv}{dx}\right) x_n \hat{k}\ .$$

This model corresponds to the situation sketched in Fig. 3 if

$$\left(\frac{dv}{dx}\right) = (5\ \mu\text{m/s})\ /\ 50\ \mu\text{m} = 0.1/\text{s}\ .$$

The complex scattered field is given by

$$E_s(t) = \sum_{n=1}^{N} A_n \exp\,[[i\mathbf{K} \cdot \mathbf{R}_n(t) - i\omega_0 t],$$

where ω_0 is the frequency of the incident light and

$$\mathbf{R}_n(t) = \mathbf{R}_n(0) + v_n t\hat{k} = \mathbf{R}_n(0) + \left(\frac{dv}{dx}\right) x_n t\hat{k}\,.$$

The unnormalized field autocorrelation function is

$$\begin{aligned} G^{(1)}[\tau] &= \langle E_s^*(t) E_s(t+\tau)\rangle \\ &= |A|^2 \exp\,[-i\omega_0\tau]\cdot \\ &\sum_{m=1}^{N}\sum_{n=1}^{N} \exp\,\{i\mathbf{K}\cdot[\mathbf{R}_n(0) - \mathbf{R}_m(0)]\}\,\langle \exp\,[iK_z(v_n - v_m)t]\rangle \exp\,[iK_z v_n \tau] \\ &= |A|^2 \exp\,[-i\omega_0\tau]\left\{\sum_{n=1}^{N} \exp\,[iK_z v_n\tau]\right. \\ &\quad \left. + \sum_{m\neq n}^{N}\sum^{N} \exp\,\{i\mathbf{K}\cdot[\mathbf{R}_n(0) - \mathbf{R}_m(0)]\}\langle \exp\,[iK_z(v_n - v_m)t]\rangle \exp\,[iK_z v_n\tau]\right\}. \end{aligned}$$

The first sum, the sum of self terms, is of order N ($\sim N$), and for large N can be approximated by an integral,

$$\sum_{n=1}^{N} \exp\,[iK_z v_n\tau] \simeq N\int_{-v_M}^{+v_M} \exp\,[iK_z v\tau]\,P(v)\,dv,$$

where $P(v)dv$ is the fraction of scatterers with velocity between v and $v + dv$, and $\pm v_M$ are the maximum positive and negative velocities of scatterers. For a cylinder with circular cross section

$$P(v)dv = 2[v_M^2 - v^2]^{1/2}dv/\pi v_M^2,$$

where $v_M = a(dv/dx)$ and a is the radius of the cylinder. Then

$$\begin{aligned} \sum_{n=1}^{N} \exp\,[iK_z v_n\tau] &\simeq N\int_{-v_M}^{+v_M} 2[v_M^2 - v^2]^{1/2} \exp\,[iK_z v\tau]\,dv/\pi v_M^2 \\ &= 2NJ_1\left[aK_z\left(\frac{dv}{dx}\right)\tau\right]\Big/\left[aK_z\left(\frac{dv}{dx}\right)\tau\right], \end{aligned}$$

where J_1 is the Bessel function of order one.

Next consider the double sum, the sum of cross terms, in the expression for $G^{(1)}[\tau]$. Since any dimension of the scattering volume is large compared with the reciprocal of the scattering vector, $\mathbf{K}\cdot[\mathbf{R}_n(0) - \mathbf{R}_m(0)]$ assumes values uniformly over many multiples of 2π, and hence

$$\sum_{m\neq n}^{N}\sum^{N} \exp\,[i\mathbf{K}\cdot[\mathbf{R}_n(0) - \mathbf{R}_m(0)] \sim N.$$

The time average term is

$$\langle \exp\,[iK_z(v_n - v_m)t]\rangle = \frac{1}{T}\int_0^T \exp\,[iK_z(v_n - v_m)t]dt \sim 1/[K_z(v_n - v_m)T],$$

where T is the experiment duration. For a scattering angle of 30° ($K_z = 8.6\ \mu m^{-1}$), a typical velocity difference of 1 μm/s, and an experiment duration of 4.8 s, $K_z(v_n - v_m)T \simeq 40$. Hence the cross terms are more than an order of magnitude smaller than the self terms and can be neglected.

The normalized field autocorrelation function is given by

$$g^{(1)}[\tau] = G^{(1)}[\tau]/G^{(1)}[0] = \exp[-i\omega_0\tau]\,2J_1\left[aK_z\left(\frac{dv}{dx}\right)\tau\right]\Big/\left[aK_z\left(\frac{dv}{dx}\right)\tau\right].$$

The intensity autocorrelation function is given by

$$g^{(2)}[\tau] = 1 + |g^{(1)}[\tau]|^2,$$

when the field is a random variable with a Gaussian distribution in time. However, the motion of the scatterers is not a stochastic process, and hence $E_s(t)$ is not strictly a random variable. Nevertheless, the repeat time of $E_s(t)$ should be longer than a typical experiment duration, so that $E_s(t)$ can be regarded as a random variable for present purposes. The randomly distributed initial phases, $\mathbf{K} \cdot \mathbf{R}_n(0)$, in the expression

$$E_s(t) = A\sum_{n=1}^{N} \exp[i\mathbf{k} \cdot \mathbf{R}_n(0)] \exp[iK_z v_n t - i\omega_0 t]$$

result in a Gaussian distribution for $E_s(t)$ (28). Hence

$$g^{(2)}[\tau] - 1 = \left\{2J_1\left[aK_z\left(\frac{dv}{dx}\right)\tau\right] \Big/ \left[aK_z\left(\frac{dv}{dx}\right)\tau\right]\right\}^2.$$

From a table of values for J_1 the half time is found to satisfy the relation

$$aK_z\left(\frac{dv}{dx}\right)\tau_{1/2} = 1.62\,.$$

The rms velocity for a cylinder with circular cross section is

$$\sigma_v = \left[\int_{-v_M}^{+v_M} v^2 P(v)\,dv\right]^{1/2} = \left(\frac{dv}{dx}\right)\frac{a}{2},$$

resulting in the relation

$$\sigma_v = 0.81/K_z\tau_{1/2} \qquad [\text{semicircular } P(v)]\,.$$

The rms velocity for a half time of 70 ms at a scattering angle of 30° ($K_z = 8.6\ \mu m^{-1}$) is 1.3 μm/s. For a 100-μm diam cylinder, $(dv/dx) = 0.05/s$.

Although the time dependence of $g^{(2)}[\tau]$ is determined by the shape of the cylinder cross section [the functional form of $P(v)$], the relation between σ_v and $K_z\tau_{1/2}$ is rather insensitive to the choice of cross section [$P(v)$]. For example, a flat or triangular $P(v)$ results in

$$\sigma_v = 0.80/K_z\tau_{1/2} \quad [\text{flat } P(v)]$$

$$\sigma_v = 0.82/K_z\tau_{1/2} \quad [\text{triangular } P(v)].$$

APPENDIX D

Model Calculation of $g^{(2)}[\tau]$: Elongation Model

Consider a model situation in which there are a large number, N, of identical Rayleigh scatterers positioned randomly throughout a cylindrical scattering volume (e.g., a segment of a muscle fiber). The

scatterers possess constant velocities along the cylinder axis (z axis) which is perpendicular to the incident beam (traveling in the positive y direction) and contained in the scattering plane (y-z plane). Let the velocity of the n^{th} scatterer be given by

$$\mathbf{v}_n = v_n\hat{k} = bz_n(0)\,\hat{k},$$

where b can be regarded as a constant rate of elongation. The position of the n^{th} scatterer is therefore given by

$$\mathbf{R}_n(t) = \mathbf{R}_n(0) + v_n t\hat{k} = \mathbf{R}_n(0) + bz_n(0)t\hat{k}\,.$$

Following a procedure identical to that outlined in Appendix C,

$$g^{(2)}[\tau] - 1 = \left| \frac{1}{N}\sum_{n=1}^{N} \exp\,[iK_z bz_n(0)\tau] \right|^2.$$

For large N the sum can be approximated by an integral,

$$\frac{1}{N}\sum_{n=1}^{N} \exp\,[iK_z bz_n(0)\tau] \simeq \int_{-\infty}^{+\infty} w(z) \exp\,[iK_z bz\tau]\mathrm{d}z,$$

where $w(z)$ is a weighting function which takes into account the diffraction pattern of the front aperture. Note that the calculations for this elongation model are independent of the shape of the cross section of the cylinder. For a very large front aperture,

$$w(z) = f(z) = \frac{1}{L} \quad -\frac{L}{2} < Z < \frac{L}{2}$$

$$= 0 \quad \text{otherwise,}$$

where $L = 3w/4 \cos\theta$, and w is the width of the rear slit. When the diameter of the front aperture is < 1 mm, $w(z)$ is the convolution of $f(z)$ with $h(z)$, where $h(z)$ was taken to be a Gaussian function with a standard deviation

$$\sigma = 0.433\,\lambda/\mathrm{d}(20\text{ cm}).$$

The model points plotted in Fig. 6 were calculated by computer for a given scattering angle, configuration of the detection optics, and rate of elongation.

REFERENCES

1. HUXLEY, A. F., and R. NIEDERGERKE. 1954. Interference microscopy of living muscle fibres. *Nature (Lond.).* **173**:971–973.
2. HUXLEY, H. E., and J. HANSON. 1954. Changes in the cross-striations of muscle during contraction and stretch and their structural interpretation. *Nature (Lond.).* **173**:973–976.
3. HUXLEY, A. F. 1957. Muscle structure and theories of contraction. *Prog. Biophys. Chem.* **7**:255–318.
4. HUXLEY, H. E., and W. BROWN. 1967. The low angle x-ray diagram of vertebrate striated muscle and its behaviour during contraction and rigor. *J. Mol. Biol.* **30**:383–434.
5. ELLIOTT, G. F., J. LOWY, and B. M. MILLMAN. 1967. Low angle x-ray diffraction studies of living striated muscle during contraction. *J. Mol. Biol.* **25**:31–45.
6. GORDAN, A. M., A. F. HUXLEY, and F. J. JULIAN. 1966. The variation in isometric tension with sarcomere length in vertebrate muscle fibres. *J. Physiol. (Lond.).* **184**:170–192.
7. GORDAN, A. M., A. F. HUXLEY, and F. J. JULIAN. 1966. Tension development in highly stretched vertebrate muscle fibres. *J. Physiol. (Lond.).* **184**:143–169.
8. BOREJDO, J., and M. F. MORALES. 1977. Fluctuations in tension during contraction of single muscle fibers. *Biophys. J.* **20**:315–334.

9. BOREJDO, J., S. PUTNAM, and M. F. MORALES. 1979. Fluctuations in polarized fluorescence: evidence that muscle cross bridges rotate repetitively during contraction. *Proc. Natl. Acad. Sci. U.S.A.* **76**:6346–6350.
10. BONNER, R. F., and F. D. CARLSON. 1975. Structural dynamics of frog muscle during isometric contraction. *J. Gen. Physiol.* **65**:555–581.
11. CARLSON, F. D. 1975. Structural fluctuations in the steady state of muscular contraction. *Biophys. J.* **15**:633–649.
12. CUMMINS, H. Z., F. D. CARLSON, T. HERBERT, and G. WOODS. 1969. Translational and rotational diffusion constants of tobacco mosaic virus from Rayleigh linewidths. *Biophys. J.* **9**:518–546.
13. CUMMINS, H. Z., and H. SWINNEY. 1970. Light beating spectroscopy. *Prog. Opt.* **8**:135–200.
14. CUMMINS, H. Z., and E. R. PIKE, editors. 1974. Photon Correlation and Light Beating Spectroscopy. Plenum Press, New York.
15. CUMMINS, H. Z., and E. R. PIKE, editors. 1977. Photon Correlation Spectroscopy and Velocimetry. Plenum Press, New York.
16. BERNE, B. J., and R. PECORA. 1976. Dynamic Light Scattering. John Wiley and Sons, Inc., New York.
17. HUXLEY, H. E., and J. HANSON. 1957. Quantitative studies on the structure of cross-striated myofibrils. I. Investigations by interference microscopy. *Biochim. Biophys. Acta.* **33**:229–249.
18. HANSON, J., and H. E. HUXLEY. 1957. Quantitative studies on the structure of cross-striated myofibrils. II. Investigations by biochemical techniques. *Biochim. Biophys. Acta.* **23**:250–260.
19. FORD, L. E., A. F. HUXLEY, and R. M. SIMMONS. 1977. Tension responses to sudden length change in stimulated frog muscle fibers near slack length. *J. Physiol. (Lond.).* **269**:441–515.
20. KOPPEL, D. E., and D. W. SCHAEFER. 1973. Scaled photocount correlation of non-Gaussian scattered light. *Appl. Phys. Lett.* **22**:36–37.
21. JAKEMAN, E., C. J. OLIVER, E. R. PIKE, and P. N. PUSEY. 1972. Correlation of scaled photon-counting fluctuations. *J. Phys. A. Gen. Phys.* **5**:L93–L96.
22. SALEH, BAHAA. 1978. Photoelectron Statistics. Springer-Verlag Inc., New York, 375–388.
23. CARLSON, F. D., and A. B. FRASER. 1974. Dynamics of F-actin and F-actin complexes. *J. Mol. Biol.* **89**:273–281.
24. CARLSON, F. D. 1975. Letters to the editor. *J. Mol. Biol.* **95**:139.
25. FUJIME, S., T. MAEDA, and Y. UMAZUME. Structures and dynamics of muscle cells and muscle proteins studied by intensity fluctuation spectroscopy of laser light. *Proc. NATO Advanced Study Institute on Scattering Techniques Applied to Supramolecular and Non-equilibrium Systems (August 1980).* Plenum Press. In press.
26. MCLAUCHLAN, N. W. 1951. Theory of Vibrations. Dover Publications, New York.
27. ARMSTRONG, C. F., A. F. HUXLEY, and F. J. JULIAN. 1966. Oscillatory responses in frog skeletal muscle fibres. *J. Physiol. (Lond.).* **186**:26P–27P.
28. RICE, S. O. 1954. Mathematical Analysis of Random Noise. Bell System Technical Journal, vols. 23 and 24. Reprinted in Noise and Stochastic Processes. N. Wax, editor. Dover Publications, New York. 179–181.